body of the crystal. A careful examination of etch patterns also reveals that some of the pits as marked in the figure show a correlation between the two faces of the plate.

Conclusions

Although $(10\bar{1}0)$ cleavage on apatite is generally somewhat imperfect, the interferograms taken on the cleavage faces discussed here indicate that over quite large regions on this face perfect cleavage occurs. The interferogram on the etched cleavage face reveals that the etch attack is twofold: (1) attack producing general dissolution of the surface by micro-pit formation and (2) attack at isolated places indicating the sites of dislocations. Successive etching of the same face for different periods produces no new pits, but simply enlargement of existing pits. This suggests that the pits may be dislocation etch pits. This is also supported by the observation of correlated pits on matched pairs of faces. The calculations made on the stratigraphical etch pattern from its displacement while crossing large cleavage steps and the corresponding step height indicate the deposition of some weak planes on the $(10\bar{1}1)$ dome faces of the crystal during growth. When the crystal is cleaved and etched, the edges of these layers form rectilinear patterns on the $(10\bar{1}0)$ faces, which are preferentially attacked during etching, thus producing the stratigraphical pattern observed. The correlation in the etch pattern on the two sides of a 1·8 mm thick plate suggests that the weak planes run right through the body of the crystal.

The authors take this opportunity to express their thanks to Dr P. B. Price of the General Electric Research Laboratory, U.S.A. for supplying apatite crystals for these investigations.

References

AMELINCKX, S. (1956). *Phil. Mag.* **1**, 269.
DANA, E. S. (1963). *A Text Book of Mineralogy*, p. 704. New York: John Wiley.
GILMAN, J. J. & JOHNSTON, W. J. (1956). *J. Appl. Phys.* **27**, 1018.
HONESS, A. P. (1927). *The Nature, Origin and Interpretation of Etch Figures on Crystals.* New York: John Wiley.
KEITH, R. E. & GILMAN, J. J. (1960). *Acta Metallurg.* **8**, 1.
LOVELL, L. C. (1958). *Acta Metallurg.* **6**, 775.
MENDELSON, S. (1961). *J. Appl. Phys.* **32**, 1579.
OSTERBURG, H., BENNET, A. H., JUPNIK, H. H. & RICHARDS, O. W. (1951). *Phase Microscopy.* New York: John Wiley.
PALACHE, C., BERMAN, H. & FRONDEL, C. (1963). *The System of Mineralogy*, p. 878. New York: John Wiley.
PATEL, A. R. & DESAI, C. C. (1964). *Z. Kristallogr.* **121**, 55.
PATEL, A. R. & DESAI, C. C. (1965). *Acta Cryst.* **18**, 373.
PATEL, A. R. & GOSWAMI, K. N. (1964). *Acta Cryst.* **17**, 569.
PATEL, A. R. & RAMANATHAN, S. (1962). *Acta Cryst.* **15**, 860.
PATEL, A. R. & TOLANSKY, S. (1957). *Proc. Roy. Soc.* A, **243**, 41.
PRICE, P. B., SYMES, E. M. & FLEISCHER, R. L. (1964). *Amer. Min.* **49**, 794.
TOLANSKY, S. (1948). *Multiple Beam Interferometry of Surfaces and Films.* Oxford: Clarendon Press.
TOLANSKY, S. (1952). *Z. Electrochem.* **56**, 263.

Acta Cryst. (1966). **20**, 798

X-Ray Diffraction Study of Cold-Worked α Ag–Cd Alloys

S. P. SENGUPTA AND M. A. QUADER
Indian Association for the Cultivation of Science, Calcutta 32, *India*

(*Received* 23 *August* 1965)

The Geiger counter X-ray diffractometer has been employed for the study of line profiles from cold-worked silver–cadmium alloys in the solid solution range. Stacking fault densities α and β have been obtained from measurements of peak-shift and peak asymmetry and a linear dependence of deformation fault probability α with solute concentration has been observed. Warren & Averbach's method of Fourier analysis of line shapes has been used for the evaluation of effective particle sizes $[D_e]_{hkl}$ and root mean square strains $[\langle \varepsilon_L^2 \rangle]_{hkl}^{\frac{1}{2}}$ and it has been found that both are anisotropic in nature and vary with increasing solute content. The importance of faulting in the particle size broadening is also clearly observed.

Introduction

The study of cold-worked metals and alloys by X-ray diffraction is important as it reveals a fairly detailed picture of the deformed state. According to X-ray study cold-work is known to cause broadening of X-ray powder diffraction line profiles, and it is generally agreed to-day that the broadening in f.c.c. metals and alloys results from a reduction in the size of the coherently diffracting domains, from distortion within these coherent domains and from stacking faults on (111) planes. In addition to line broadening, peak-shift and peak

asymmetry are also observed in many cases and are due to deformation and twin stacking faults respectively (Warren, 1959). Besides these, spacing faults may also introduce additional line broadening and peak-shift, as has been shown by Wagner, Tetelman & Otte (1962).

The occurrence of stacking faults in cold-worked Ag–Cd alloys in the solid-solution range was first reported by Davies & Cahn (1962) and subsequently by Adler & Wagner (1962) and Vassamillet & Massalski (1963). In all these measurements it has been observed that deformation fault probability α increases with increasing cadmium content in accordance with other silver-base alloys (Vassamillet, 1961; Mikkola & Cohen, 1962; Sundahl & Sivertsen, 1963). X-ray studies of binary alloys based on the noble metals copper and gold have also shown the pronounced increase in stacking fault probability with increasing solute concentration (*e.g.* Warren & Warekois, 1955; Wagner, 1957; Smallman & Westmacott, 1957; Christian & Spreadborough, 1957; Bolling, Massalski & McHargue, 1961; Foley, Cahn & Raynor, 1963; Vassamillet & Massalski, 1964). Adler & Wagner (1962), in their studies, have further investigated the sources of line broadening in Ag–Sn and Ag–In alloy systems.

In the present investigation on filings of α-phase silver-cadmium alloys, besides the determination of stacking fault parameters, line broadening studies have been carried out following Warren & Averbach's method (Warren, 1959) of Fourier analysis of line shapes with a view to obtaining information regarding (i) the nature of particle sizes and strain distributions in the deformed condition, (ii) the role of different contributors in the observed line broadening effect, and (iii) the effect of solute concentration on the different parameters.

Experimental results

Sample preparation and experimental procedure

The alloys used in this study were prepared from spectroscopically pure silver and cadmium rods supplied by Messrs Johnson, Matthey and Co. Ltd., London. Accurately weighed quantities of the component metals, sufficient to give 8-g ingots, were melted together in an evacuated and sealed quartz capsule; after melting, the alloys were homogenized for 10 days in the range 700–750 °C. Weight changes during preparation were negligible. Five different alloys of silver-cadmium of varying cadmium content were prepared in the solid-solution range.

Cold working was achieved by hand filing at room temperature. Out of the filings, one sample was retained in the 'as-filed' condition and the other was annealed at 600 °C for 4 hours in a Pyrex glass capsule sealed under vacuum. After sieving through a 250 mesh screen, specimens of filings were bonded with a solution of Canada balsam in xylene and mounted in a specially designed aluminum plate holder which could itself be mounted in the specimen position in the diffractometer. The filings presented an accurately flat surface (20 × 12 mm) to the X-ray beam. The line profiles were recorded with the standard Philips Geiger counter X-ray diffractometer (PW1050, 1051) with nickel filtered Cu $K\alpha$ radiation from a highly stabilized X-ray generator (PW1010). Accurate line profiles of the reflexions were obtained by point counting at intervals of 0·05° in 2θ for the general background, decreasing to 0·01° in 2θ near the maxima of the peaks, where θ is the Bragg angle. All the measurements were done at room temperature (25 ± 1 °C).

Estimation of stacking faults

Measurement of peak position leads to a direct determination of the deformation fault probability. Thus, the fault probability α is obtained form the change in separation of 111 and 200 reflexions using the relation (Wagner, 1957):

$$(2\theta^{\circ}_{hkl}-2\theta^{\circ}_{h'k'l'})_{\mathrm{CW}}-(2\theta^{\circ}_{hkl}-2\theta^{\circ}_{h'k'l'})_{\mathrm{Ann}}=H\,.\,\alpha \qquad (1)$$

and

$$H=(\langle G\rangle j\,.\,\tan\theta^{\circ})_{hkl}-(\langle G\rangle j\,.\,\tan\theta^{\circ})_{h'k'l'}\,, \qquad (2)$$

where j is the fraction of (hkl) planes affected by deformation faults, $G=(\pm)\,90|/3\,.\,h_3/\pi^2 l_0^2$ and $\langle G\rangle$ is the averaged value for the hkl reflexions affected by deformation faults.

The peak positions were obtained by the method of mid-point extrapolation of chords parallel to background level to peak maximum. The estimated accuracy of the position measurements was about ±0·01° in 2θ. Elimination of the α_2 component in case of cold-worked peaks was not possible since the graphical methods of Rachinger (1948) and of Papoulis (1955) could not be applied for broad, overlapping and asymmetric line profiles. Also, because of statistical fluctuations, point of maximum intensity cannot be taken as a position for peak maximum.

Twin faults asymmetrically broaden the diffraction line profiles. A method of determining twin fault probability β based on the displacement of the centre of gravity of a peak from the peak maximum has been developed by Cohen & Wagner (1962). By combining Δ C.G. ($^{\circ}2\theta$), the displacement of the centre of gravity from the peak maximum, for 111 and 200 reflexions partial compensation for systematic and instrumental effects can be achieved. The displacements of 111 and 200 peaks are related to β as:

$$\Delta\ \mathrm{C.G.}\ (^{\circ}2\theta)_{111}=+11\ \beta\ \tan\theta_{111} \qquad (3)$$

$$\Delta\ \mathrm{C.G.}\ (^{\circ}2\theta)_{200}=-14{\cdot}6\ \beta\ \tan\theta_{200}\,. \qquad (4)$$

For the determination of the C.G. of the line profiles, the method of Ladell, Parrish & Taylor (1959) has been adopted. Prior to actually evaluation of the C.G., each peak height was divided by the factor (Warren, 1959) $f^2(1+\cos^2 2\theta)/\sin^2\theta$, where f is the atomic scattering factor. However, experimental limitations (such as long tails, peak overlap and error in peak maximum position determination) do not enable us to obtain Δ C.G. accurately and hence a good accuracy in values of β.

Values of α and β are given in Table 1, and Fig. 1 shows the dependence of α with solute concentration, as observed by us and by other workers.

Line shape analysis

Fourier analysis of line shapes provides information about the effective particle size, the strain distribution and the compound fault probability ($1{\cdot}5\alpha+\beta$). The 111, 222, 200 and 400 reflexions were chosen, as with these it is possible to determine particle sizes and lattice strains in [111] and [100] directions. Initially, Stokes's (1948) method was used for correcting for instrumental broadening. It has been assumed that line shapes obtained from the samples annealed for 4 hours at 600 °C are an exact measure of instrumental broadening. Fourier coefficients expressing the line shapes were obtained by means of Beevers–Lipson strips (Beevers, 1952). The corrected coefficients were represented as A_L *versus* L where L ($=na_3$) has the significance of a distance normal to the reflecting planes. To separate the effect of strain and particle size on the broadening, the Warren–Averbach method (Warren, 1959) is followed.

The power distribution per unit length of a symmetrical reflexion from a cold-worked sample at any angle 2θ is represented by a cosine Fourier series:

$$P_{2\theta}=K(\theta)N\sum_n A_n(l)\cos 2\pi nh_3\,, \qquad (5)$$

where $h_3=(2a_3\sin\theta)/\lambda$ is a variable which changes continuously with θ and takes the integral value $h_3=l$ at the peak, a_3 is the interplanar spacing in the c direction of the orthorhombic lattice, while N is the total number of cells in the crystal.

The cosine coefficient A_n can be written

$$A_n(l)=A_n^P A_n^D(l)\,, \qquad (6)$$

where A_n^P (particle size coefficient) $=1/N\sum_{i=|n|+1}^{\infty}(i-|n|)n_i$ and A_n^D (distortion coefficient) $=\langle\cos 2\pi lZ_n\rangle_{\mathrm{av}}$; Z_n is defined in such a manner that a_3Z_n is the change in length of a column of original length $L=na_3$.

For a Gaussian strain distribution,

$A_L^D=\exp[-2\pi^2 l_0^2\langle\Delta L^2\rangle/a^2]$, where $l_0^2=h^2+k^2+l^2$, $a_3/l=d=a/l_0$, $\Delta L=a_3Z_n$, and a_3 is obtained from the relation $2a_3/\lambda\,.\,(\sin\theta_M-\sin\theta_0)=\frac{1}{2}$, where θ_0 is the Bragg angle at the point of maximum intensity and θ_M is the point where the tail merges with the background.

The Fourier coefficients were interpreted by plotting $\ln A_L$ against l_0^2 for various values of L. Logarithmic plots were made for the two sets of multiple orders 111 – 222 and 200 – 400. The intercepts of these curves at $l_0^2=0$ give Fourier coefficient A_L^P which is due only to particle size and stacking fault broadening. The slopes give mean square average strain components

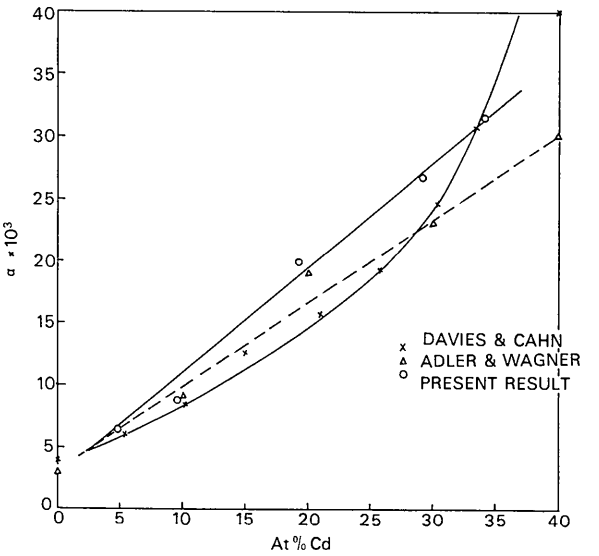

Fig. 1. Deformation fault probability α as a function of cadmium concentration.

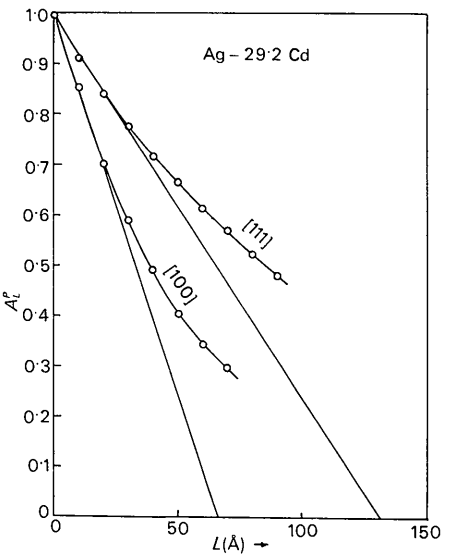

Fig. 2. Plots of particle size coefficient $A_L{}^P$ *versus* L for the [100] and [111] directions for cold-worked Ag-29.2 at. % Cd alloy. The intercepts on L of the initial slope give effective particle size $[D_e]_{hkl}$.

Table 1. *Experimental results for silver–cadmium alloys*

Composition (at. %)	$\alpha\times10^3$	$\beta\times10^3$	$[D_{SF}]_{111}$ (Å)	$[D_e]_{111}$ (Å)	$[D_e]_{100}$ (Å)	$\frac{[D_e]_{111}}{[D_e]_{100}}$	$T_{\min}$ (Å)	$[\langle\varepsilon^2_{L=50\,\text{Å}}\rangle]_{111}{}^{\frac{1}{2}}\times10^3$	$[\langle\varepsilon^2_{L=50\,\text{Å}}\rangle]_{100}{}^{\frac{1}{2}}\times10^3$	$\frac{[\langle\varepsilon^2_{L=50\,\text{Å}}\rangle]_{100}{}^{\frac{1}{2}}}{[\langle\varepsilon^2_{L=50\,\text{Å}}\rangle]_{111}{}^{\frac{1}{2}}}$
Ag– 4·8 Cd	6·5	10·2	473	208	116	1·8	328	2·5	3·2	1·3
Ag– 9·6 Cd	8·8	9·3	418	190	101	1·9	363	2·6	3·3	1·3
Ag–19·3 Cd	19·9	18·7	196	160	75	2·1	739	2·5	3·2	1·3
Ag–29·2 Cd	26·7	20·2	160	130	66	2·0	313	2·9	3·8	1·3
Ag–34·1 Cd	31·5	35·0	120	125	60	2·1	450	2·8	3·9	1·4

$\langle \varepsilon_L^2 \rangle$ from which r.m.s. strains are obtained for [111] and [100] directions. Plots of A_P^L obtained from *hkl* reflexions are then made as a function of L, and the intercepts on L of the initial slope give the effective particle size $[D_e]_{hkl}$. The Hook effect (Warren, 1959) was not observed in the region of small L. Table 1 summarizes the values of $[D_e]_{hkl}$ and $[\langle \varepsilon^2_{L=50\,\text{Å}} \rangle]^{\frac{1}{2}}_{hkl}$ for the five compositions of the silver-cadmium system, and Figs. 2 and 3 show the plots of A_L^P and $\langle \varepsilon_L^2 \rangle^{\frac{1}{2}}$ as a function of distance L for both [111] and [100] directions in the Ag–29·2 Cd alloy. Fig. 4 illustrates the decrease in effective particle size as the amount of cadmium concentration increases.

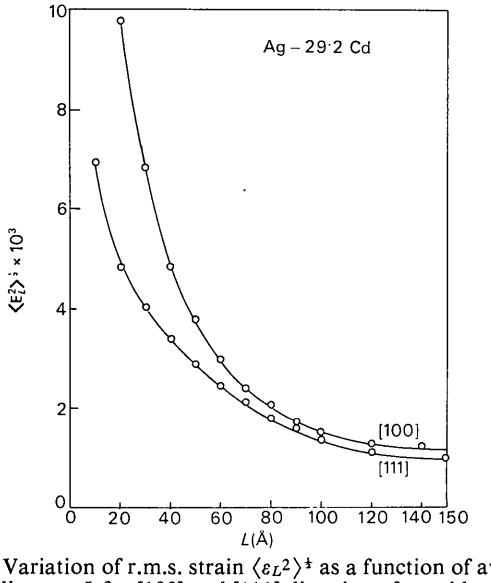

Fig. 3. Variation of r.m.s. strain $\langle \varepsilon_L{}^2 \rangle^{\frac{1}{2}}$ as a function of averaging distance L for [100] and [111] directions for cold-worked Ag–29·2 Cd alloy.

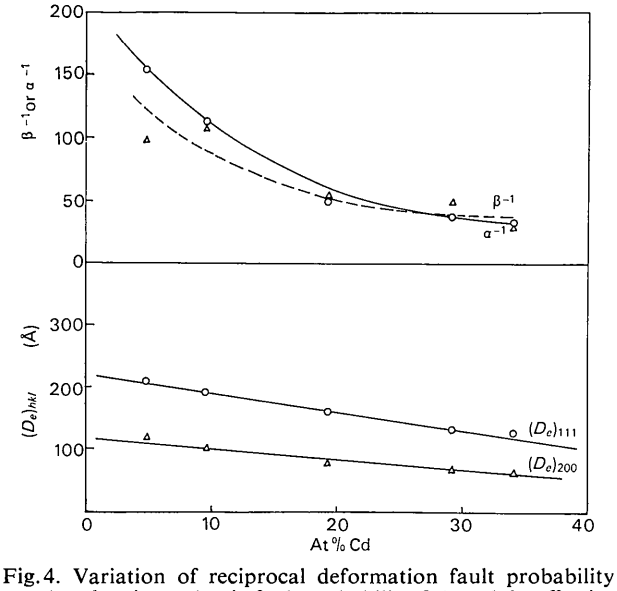

Fig. 4. Variation of reciprocal deformation fault probability α^{-1} and reciprocal twin fault probability β^{-1}, and the effective particle size in the [*hkl*] direction $(D_e)_{hkl}$ as a function of cadmium concentration.

Discussion

It is seen from Fig. 1 that deformation fault probability α increases with increasing cadmium content and α has a linear dependence with solute concentration. This linear dependence of α in Ag–Cd alloys has been also observed by the previous studies (Adler & Wagner, 1962; Vassamillet & Massalski, 1963). Davies & Cahn (1962) have obtained a roughly parabolic plot, the deviation from linearity being pronounced at higher solute concentration. In fact, their results for other Ag-base alloys deviate also from those of Adler & Wagner (1962) and Vassamillet & Massalski (1963). This cannot be due to the difference in technique since Vassamillet & Massalski (1963) obtained the values of α from shifts of peak centroids and the values are also much larger. However, a close examination of the figure shows that values of α obtained from the present investigation lie close to those reported by Davies & Cahn (1962) and Adler & Wagner (1962), and for the differences in magnitudes and slopes observed in these cases the factors peak maximum determinations and differences in filing temperatures (Vassamillet & Massalski, 1963) are to be considered. As seen from Table 1, twin fault probability β has been also found to increase with composition, but since the method of obtaining β suffers from experimental limitations systematic variations are not observed in the present case.

The anisotropy of effective particle sizes and lattice strains has been clearly observed. Warren (1961) has shown that the effective particle size may be written in terms of the coherently diffracting domain size D normal to the reflecting planes, the deformation and twin fault probabilities α and β, the domain size T in the faulting plane and the lattice parameter a:

$$\frac{1}{[D_{\text{eff}}]_{111}} = \frac{1}{D} + \frac{1}{\sqrt{2}T} + \frac{1{\cdot}5\alpha+\beta}{a}\,\frac{\sqrt{3}}{4} \tag{7}$$

$$\frac{1}{[D_{\text{eff}}]_{100}} = \frac{1}{D} + \frac{1}{\sqrt{1{\cdot}5}\,T} + \frac{1{\cdot}5\alpha+\beta}{a}. \tag{8}$$

The inverse of the last term is referred to as D_{SF}, the fictitious domain size due to faulting. It has been also shown by Warren (1961) that a minimum value of T is given by:

$$T_{\min} = \frac{0{\cdot}82}{\dfrac{2{\cdot}31}{[D_e]_{111}} - \dfrac{1}{[D_e]_{100}}}. \tag{9}$$

Now it is observed from Fig. 4 that both the effective particle size and the reciprocal stacking fault probability decrease with the increase of cadmium concentration, and this implies that stacking faults do contribute significantly to the observed particle size broadening. This is further supported by the fact that observed values of $[D_e]_{111}/[D_e]_{100}$ are very close to the theoretically predicted values of 2·3 for $[D_e]_{111}/[D_e]_{100}$ and the computed values of $[D_{SF}]$ agree fairly well with $[D_e]$ obtained from line broadening (Table 1). The influence

of D and also T (as appears from the values of T_{min}) on the magnitude of D_{eff} seems to be small so that the stacking faults may be thought of as being completely extended across a coherent domain dimension D. A significant contribution of stacking faults to particle size broadening has been also observed in Ag–In and Ag–Sn alloys (Adler & Wagner, 1962).

The strains seem to vary rapidly with distance in the material for small L values, whereas for increasing distance normal to the reflecting planes the change is small (Fig. 3). The same nature was exhibited by all the specimens in both directions. The decrease with increasing L might be due to the fact that strains are highly inhomogeneous. The trend of the curve at higher L can be explained by considering some regions of positive and negative strains lying close together which produce some sort of cancelling effect when averaged over longer distances. The values of r.m.s. strains at an averaging distance $L = 50$ Å are tabulated in Table 1 and a gradual increase is observed with solute concentrations. But the increase in either direction is not so pronounced at higher solute concentration as compared with other silver base alloys (Fig. 5). This may be explained by considering the effect of addition of polyvalent solutes to a monovalent solvent metal. Plotting α as a function of electron concentration e/a, it has been observed that the addition of polyvalent solutes Cd^{2+}, In^{3+}, Sn^{4+} to Ag increases the deformation fault probability α in the order Ag–Cd, Ag–In, Ag–Sn (Fig. 6) and consequently the higher density of dislocations which in turn give rise to the additional amount of strain found in the Ag–Sn system (Adler & Wagner, 1962). The strain values are anisotropic, as is expected from the differences in Young's modulus in these directions. The ratio of r.m.s. strains measured at $L = 50$ Å and also averaged over the distance L from 30 Å to 100 Å is about 1·3. However, this observed anisotropy of strain cannot be accounted for by the simple isotropic stress model according to which the residual microstrains in the [*hkl*] direction will be inversely proportional to the directional Young's modulus. Using elastic constants data of silver and also of dilute silver–cadmium alloys (Bacon & Smith, 1956), as the literature shows no such measurements in the solid solution range, it turns out that $E_{[111]}/E_{[100]} = 2{\cdot}7$. Thus, it can only be inferred that the observed anisotropy of strain is probably related to the non-uniform distribution of dislocations and to the stress directionality (Cottrell, 1953) of dislocations and stacking faults.

The authors are grateful to Prof. B. N. Srivastava for his continued interest in the work.

References

Adler, R. P. I. & Wagner, C. N. J. (1962). *J. Appl. Phys.* **33**, 3451.

Bacon, R. & Smith, C. S. (1956). *Acta Metallurg.* **4**, 337.

Beevers, C. A. (1952). *Acta Cryst.* **5**, 670.

Bolling, G. F., Massalski, T. B. & McHargue, C. J. (1961). *Phil. Mag.* **6**, 491.

Christian, J. W. & Spreadborough, J. (1957). *Proc. Phys. Soc. Lond.* B **70**, 1151.

Cohen, J. B. & Wagner, C. N. J. (1962). *J. Appl. Phys.* **33**, 2073.

Cottrell, A. H. (1953). *Dislocation and Plastic Flow in Crystals*, Ch. III, p. 73. Oxford: Clarendon Press.

Davies, R. G. & Cahn, R. W. (1962). *Acta Metallurg.* **10**, 621.

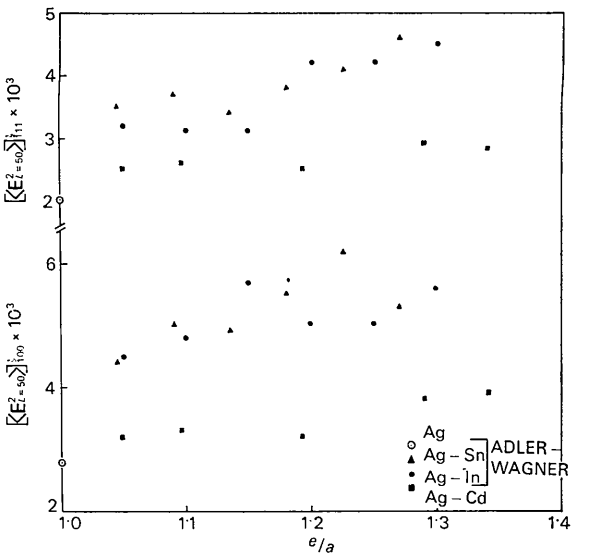

Fig. 5. Variation of r.m.s. strain $[\langle \varepsilon^2_{L=50\,\text{Å}} \rangle]^{\frac{1}{2}}$ as a function of electron concentration e/a for [100] and [111] directions for cold-worked silver-base alloys.

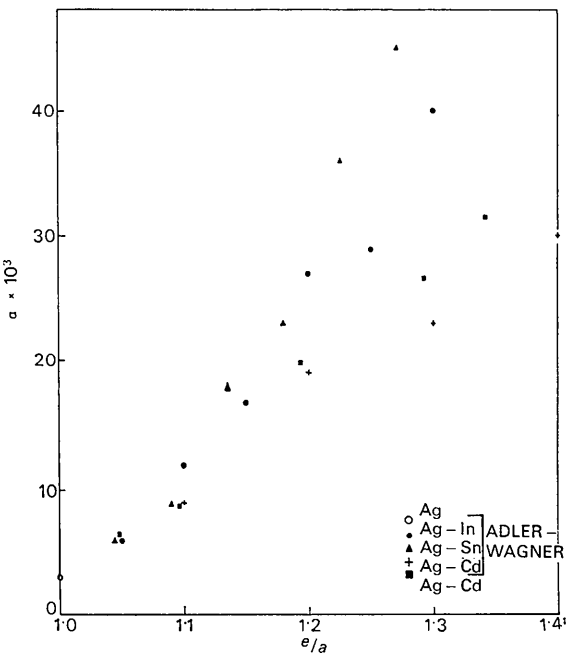

Fig. 6. Deformation fault probability α as a function of electron concentration e/a in silver-base alloys.

FOLEY, J. H., CAHN, R. W. & RAYNOR, G. V. (1963). *Acta Metallurg.* **11**, 355.
LADELL, J., PARRISH, W. & TAYLOR, J. (1959). *Acta Cryst.* **12**, 253.
MIKKOLA, D. E. & COHEN, J. B. (1962). *J. Appl. Phys.* **33**, 892.
PAPOULIS, A. (1955). *Rev. Sci. Instrum.* **26**, 423.
RACHINGER, W. A. (1948). *J. Sci. Instrum.* **25**, 254.
SMALLMAN, R. E. & WESTMACOTT, K. H. (1957). *Phil. Mag.* **17**, 669.
STOKES, A. R. (1948). *Proc. Phys. Soc., London,* B **61**, 382.
SUNDAHL, R. C. & SIVERTSEN, J. M. (1963). *J. Appl. Phys.* **34**, 994.
VASSAMILLET, L. F. & MASSALSKI, T. B. (1963). *J. Appl. Phys.* **34**, 3398. (1964). *J. Appl. Phys.* **35**, 2629.
VASSAMILLET, L. F. (1961). *J. Appl. Phys.* **32**, 778.
WAGNER, C. N. J., TETELMAN, A. S. & OTTE, H. M. (1962). *J. Appl. Phys.* **33**, 3080.
WAGNER, C. N. J. (1957). *Acta Metallurg.* **5**, 427.
WARREN, B. E. (1959). *Progr. Metal Phys.* **8**, 147.
WARREN, B. E. (1961). *J. Appl. Phys.* **32**, 2428.
WARREN, B. E. & WAREKOIS, E. P. (1955). *Acta Metallurg.* **3**, 473.

Acta Cryst. (1966). **20**, 803

The Crystal Structure of Di-μ-hydroxobis(dimethylaminecopper (II)) Sulfate Monohydrate

BY YOICHI IITAKA, KAZUO SHIMIZU* AND TAKAO KWAN

Faculty of Pharmaceutical Sciences, University of Tokyo, Hongo, Tokyo, Japan

(*Received* 1 *September* 1965)

The crystal structure of di-μ-hydroxobis(dimethylaminecopper(II)) sulfate monohydrate, $Cu_2(NH_2CH_3)_4(OH)_2SO_4 . H_2O$, has been determined by X-ray analysis. The crystals are triclinic with space group $P\bar{1}$ and the cell dimensions are, $a=9{\cdot}28_1$, $b=11{\cdot}31_1$, $c=7{\cdot}42_5$ Å, $\alpha=98{\cdot}6_8$, $\beta=92{\cdot}9_4$, $\gamma=113{\cdot}1_9°$, with two formula units in the cell. The final parameters were evaluated by a full-matrix least-squares treatment of three-dimensional data.

The structure contains two crystallographically independent copper(II) atoms having a tetragonal pyramidal coordination. Each copper atom is coordinated by two hydroxyl anions and two nitrogen atoms of methylamine to form a binuclear complex ion. The two hydroxyl ions are shared by the two copper atoms. The complex ion is puckered at the hydroxyl ions and this results in a rather close approach, 2·78 Å, between the copper atoms. Two such complex ions are bound together to form a dimer, in which the hydroxyl ion in one of the complex ions is coordinated as a fifth ligand to the copper atom in the other. A water molecule is coordinated to another copper atom of the complex ion as a fifth ligand. The dimers are piled up along the *c* axis, and sulfate ions are attached to them through hydrogen bonds. These columnar units of the structure are packed together parallel to the *c* axis to complete the structure.

Experimental

In the course of a study of the hydrogenation catalysis by cupric salts dissolved in organic bases, a new compound with the composition $Cu_2(NH_2CH_3)_4(OH)_2SO_4 . H_2O$ was found to deposit in reaction flasks. In view of the significance of the structural correlation of this complex with the substrate, a structural analysis was undertaken on it by X-ray diffraction.

The complex was prepared by dissolving $CuSO_4 . 5H_2O$ in a 40% aqueous solution of methylamine in a water bath with a molar ratio of copper to methylamine 1:4. After filtration of the dark blue solution obtained, a small amount of alcohol was added to it. The solution was then suddenly cooled to liquid nitrogen temperature in order to stimulate crystallization. Many small crystals were obtained as a precipitate when the solution was kept in a refrigerator for a while. The crystal suitable for the X-ray work was grown from the solution at room temperature by using a crystal from the precipitate as a seed crystal.

The crystals collected were dark blue, elongated along the *c* axis, and often twinned with the twinning axis *c*. The crystals were unstable and easily decomposed on exposure to the air. During the exposure to X-rays, the specimen was kept in a thin-walled Pyrex glass capillary filled with methylamine and ethyl alcohol vapours. Although the results of chemical analysis showed poor reproducibility because of such instability of the specimen, the molar proportions of copper, methylamine, sulfate and water were found to be approximately 2:4:1:3, where the water content was determined by Karl Fischer's method. In the course of the structure determination, it became clear that two of the three 'water molecules' determined by Karl Fischer's method

* Present address: The Government Chemical Industrial Research Institute, Tokyo, Shibuya-ku, Tokyo, Japan.